

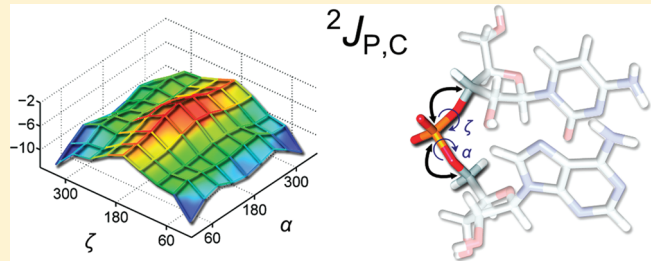
Correlating the ^{31}P NMR Chemical Shielding Tensor and the $^2J_{\text{P},\text{C}}$ Spin–Spin Coupling Constants with Torsion Angles ζ and α in the Backbone of Nucleic Acids

Ladislav Benda,* Zuzana Sochorová Vokáčová, Michal Straka, and Vladimír Sychrovský*

Institute of Organic Chemistry and Biochemistry, Academy of Sciences of the Czech Republic, v.v.i., Flemingovo náměstí 2, 166 10 Prague 6, Czech Republic

Supporting Information

ABSTRACT: Determination of nucleic acid (NA) structure with NMR spectroscopy is limited by the lack of restraints on conformation of NA phosphate. In this work, the ^{31}P chemical shielding tensor, the $\Gamma_{\text{P},\text{CSHS}1}$ and $\Gamma_{\text{P},\text{CSHS}2}$ cross-correlated relaxation rates, and the $^2J_{\text{P},\text{C}3}$, $^2J_{\text{P},\text{C}5}$, and $^3J_{\text{P},\text{C}4}$ coupling constants were calculated in dependence on NA backbone torsion angles ζ and α . While the orientation of the ^{31}P chemical shielding tensor was almost independent of the NA phosphate conformation, the principal tensor components varied by up to ~ 40 ppm. This variation and the dependence of the phosphate geometry on torsion angles ζ and α had only a minor influence on the calculated $\Gamma_{\text{P},\text{CSHS}1}$ and $\Gamma_{\text{P},\text{CSHS}2}$ cross-correlated relaxation rates, and therefore, the so-called rigid tensor approximation was here validated. For the first time, the $^2J_{\text{P},\text{C}}$ spin–spin coupling constants were correlated with the conformation of NA phosphate. Although each of the two J -couplings was significantly modulated by both torsions ζ and α , the $^2J_{\text{P},\text{C}3}$ coupling could be structurally assigned to torsion ζ and the $^2J_{\text{P},\text{C}5}$ coupling to torsion α . We propose qualitative rules for their structural interpretation as loose restraints on torsion angles ζ and α . The $^3J_{\text{P},\text{C}4}$ coupling assigned to torsion angle β was found dependent also on torsions ζ and α , implying that the uncertainty in determination of β with standard Karplus curves could be as large as $\sim 25^\circ$. The calculations provided a unified picture of NMR parameters applicable for the determination of NA phosphate conformation.



INTRODUCTION

The biological function of nucleic acids (NAs) is closely related to their three-dimensional architecture, which is determined by the geometry of the NA backbone. The NA backbone consists of chemically identical segments appearing repetitively along the NA strand (Figure 1a). Although full rotational freedom of NA backbone torsion angles ε , ζ , α , β , γ , and δ would correspond to a rather extreme number of hypothetical conformers, the backbone geometries were shown to cluster only into a relatively small number of distinguished structural patterns.¹ These so-called NA conformational classes determined both for DNA and RNA molecules in crystals² are nowadays used for classification of NA backbone geometries. While the DNA molecules predominantly occur in A-, B_1 , B_{11} , and Z-form, the conformational richness of RNA molecules is described with 46 conformational classes.¹

Nuclear magnetic resonance (NMR) spectroscopy has become an indispensable technique in structural studies of NAs.^{3–6} It provides a unique alternative to X-ray crystallography, enabling to probe conformation and dynamics of NAs in their native environment. The NMR structural studies of the NA backbone utilize mainly NMR relaxation enhancements due to the nuclear Overhauser effect (NOE), residual dipolar couplings (RDCs) in partially oriented media, three-bond spin–spin coupling constants (3J -couplings), and newly also

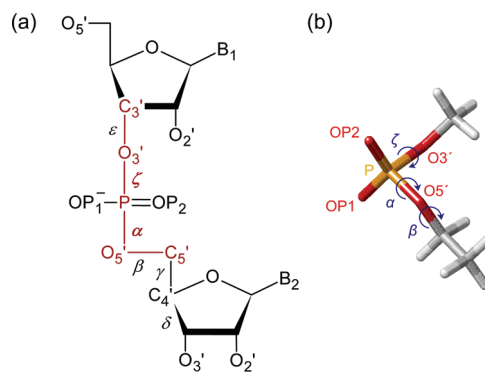


Figure 1. (a) Definition of NA backbone torsion angles. The symbols B_1 and B_2 stand for NA bases, which were in the nPn model replaced by methyl groups. (b) Ethyl methyl phosphate (EMP) with atoms and torsion angles defined in analogy to NA backbone. The nPn and EMP models of NA phosphate were used in this study for calculating the dependence of NMR parameters on torsion angles ζ and α .

Received: October 14, 2011

Revised: February 10, 2012

Published: March 1, 2012

cross-correlated relaxation (CCR) rates. The NOEs provide interatomic distances, the RDCs contain information on spatial orientation of dipolar vectors, and the 3J -couplings^{3,4,7} and the $\Gamma_{P,CH}$ CCR rates^{8,9} are interpreted as structural restraints on the NA backbone torsion angles.

The NMR measurements in the NA backbone are conditioned by the abundance of spin- $1/2$ nuclei 1H , ^{13}C , and ^{31}P . The C3'-O3'-P-OS'-CS' segment including the phosphate group is in this regard particularly difficult due to the multiple occurrences of backbone oxygen atoms (Figure 1). The torsion angles ζ and α thus cannot be determined on the basis of 3J -couplings, and alternative NMR restraints on NA phosphate conformation are needed.³ Virtually, the only available NMR parameters directly responding to the conformation of torsion angles ζ and α are the isotropic ^{31}P chemical shift δ_p , the $\Gamma_{P,CH}$ CCR rates, which are closely related to the ^{31}P chemical shielding anisotropy (CSA), and the $^2J_{P,C}$ spin–spin coupling constants. Their complex structural dependencies, however, require accurate calibration, which was the main aim of this work. It should be noted that an empirical correlation between torsions ε and ζ in NA structures is known and a combined measurement of δ_p and the $^2J_{P,H3'}$ coupling is used to restrict the value of torsion ζ .¹⁰

There are further obstacles concerning the ^{31}P NMR studies of the NA backbone. The highly uniform chemical structure of the NA backbone is manifested in a relatively narrow range of δ_p .¹¹ This fact limits the assignment and interpretation of δ_p in large NA molecules exceeding ca. 40 nucleotides. Specific interactions of metal ions with the NA phosphate may also affect the structural interpretation of ^{31}P NMR parameters.¹² The NMR determination of torsion angles ζ and α is therefore still challenging, and restraints on the (ζ, α) conformation even of a qualitative nature would help to improve the precision of NA structures.

The torsions ζ and α typically adopt one of the orientations commonly called *gauche* ($g+$, 60° or $g-$, 300°) and *trans* (t , 180°). Historically, δ_p was used as a very loose restraint on the NA backbone structure, allowing one to exclude the *trans* conformation of either torsion ζ or α if the δ_p value was within the -5 to -4 ppm range.³ Structural interpretation of the δ_p exceeding this interval was considered problematic. Early *ab initio* calculations for the dimethyl phosphate (DMP) suggested that δ_p decreases when the (ζ, α) conformation of NA phosphate changes from $(g-, g-)$ to $(t, g-)$.^{11,13} The decrease of δ_p by 1.6 ppm was actually measured and assigned to DNA conformational transition $B_I \rightarrow B_{II}$ corresponding to the $(t, g-, g-) \rightarrow (g-, t, g-)$ change of $(\varepsilon, \zeta, \alpha)$ torsion angles.¹⁰ The same δ_p difference was recently modeled by combining molecular dynamics simulations of the Dickerson–Drew dodecamer with DFT NMR calculations.¹⁴ Přečechtělová et al. also calculated the structural dependence of the ^{31}P chemical shift in the DMP model with an explicitly hydrated phosphate group, where the (ζ, α) torsions were confined around the $(g-, g-)$ and $(t, g-)$ conformations.¹⁵ Despite the effort, general rules for structural interpretation of δ_p in NA phosphate are still missing. The reason is that, besides the dependence on torsion angles ζ and α , δ_p is sensitive also to the O–P–O bond angles,^{10,11,16} torsion angles ε and β ,^{17,18} and phosphate group solvation.^{12,19}

The anisotropic components of the ^{31}P chemical shielding tensor can be exploited through their contribution to NMR relaxations. It was shown that the torsion angles ζ and α can be determined on the basis of CCR rates $\Gamma_{P,CH}$ in combination

with the 3J -couplings assigned to torsions ε and β .⁸ This approach was modified in a recent work by Schwalbe's group,⁹ where the torsion angles ζ and α were unambiguously determined by combined measurement of $\Gamma_{P,CH}$ and NOE. Structural interpretation of the $\Gamma_{P,CH}$ CCR rates usually relies on the so-called "rigid tensor approximation", which assumes that the principal components of the ^{31}P chemical shielding tensor including their orientation in the molecular frame remain the same for different phosphate geometries. The approximation usually employs the ^{31}P chemical shielding tensor measured in barium diethyl phosphate (BDEP) in the solid state.²⁰ Validity of the rigid tensor approximation in the interpretation of $\Gamma_{P,CH}$ CCR rates can be tested, e.g., by theoretical calculations of their dependencies on NA phosphate conformation.

The only remaining NMR parameters that could be used for the determination of torsion angles ζ and α are the $^2J_{P,C3'}$ and $^2J_{P,CS'}$ spin–spin coupling constants involving the carbon atoms in the closest vicinity of NA phosphate (Figure 1). While a significant modulation of $^2J_{P,C3'}$ and $^2J_{P,CS'}$ by both torsion angles ζ and α can be expected, their dependence on NA phosphate geometry has not been systematically studied yet. Our previous calculations indicated that the *gauche* and *trans* orientations of torsions ζ and α could be distinguished with ~ 2 – 3 Hz differences in magnitudes of the $^2J_{P,C3'}$ and $^2J_{P,CS'}$ couplings, respectively.⁷ Similar variation of the two $^2J_{P,C}$ couplings was actually measured in NAs, but no structural interpretation was available.^{21–25}

In this theoretical work, we therefore particularly addressed the dependencies of $^2J_{P,C}$ coupling constants on torsion angles ζ and α in order to assess their applicability for determining the NA phosphate conformation. We further studied the conformational behavior of the ^{31}P chemical shielding tensor and addressed the validity of the rigid tensor approximation commonly accepted in the interpretation of CCR rates. By this, we wish to fill the existing gap in utilization of the ^{31}P NMR parameters in structural studies of the NA backbone.

THEORY

Chemical Shielding and Chemical Shift. In this work, we consistently distinguish ^{31}P chemical shielding σ_p defined as a decrease of magnetic field at the site of the ^{31}P nucleus due to the surrounding electronic environment, $B = B_0(1 - \sigma_p)$, from the ^{31}P chemical shift δ_p , which represents the relative NMR scale defined with respect to the chemical shielding of a NMR standard σ_{std}

$$\delta_p = \frac{\sigma_{std} - \sigma_p}{1 - \sigma_{std}} \approx \sigma_{std} - \sigma_p \quad (1)$$

Accordingly, the theoretical chemical shift is obtained as a difference between chemical shielding calculated in NMR standard and in the molecule of interest. In this work, σ_p and σ_{std} were always calculated at the same level.

The usual ^{31}P NMR standard is 85% aqueous solution of phosphoric acid (H_3PO_4 (aq)). Calculation of the ^{31}P chemical shielding in H_3PO_4 (aq) is a challenging task, which can be circumvented, e.g., by introducing secondary standard PH_3 , as was suggested by van Wüllen.²⁶ The isotropic ^{31}P chemical shift in the NA phosphate is then evaluated as

$$\delta_p = -266.1 + \sigma_{PH_3} - \sigma_p \quad (2)$$

where -266.1 ppm is the experimental chemical shift of the gas-phase PH_3 relative to the 85% H_3PO_4 (aq)²⁷ and σ_{PH_3} and σ_{P} are the isotropic ^{31}P chemical shieldings calculated in the secondary standard PH_3 and in NA phosphate, respectively. If not specified otherwise, the value $\sigma_{\text{PH}_3} = 566.0$ ppm calculated with the B3LYP/IGLO-III method was used. We note that, while σ_{PH_3} was calculated in the gas phase to comply with the experimental conditions,²⁷ the calculation of σ_{P} required inclusion of water solvent effects.

Chemical Shielding Anisotropy. The ^{31}P CSA was defined as

$$\Delta\sigma_{\text{P}} = \sigma_{\text{P},33} - \frac{\sigma_{\text{P},11} + \sigma_{\text{P},22}}{2} \quad (3)$$

where $\sigma_{\text{P},11} < \sigma_{\text{P},22} < \sigma_{\text{P},33}$ are the principal components of the ^{31}P chemical shielding tensor.

CSA-DD Cross-Correlated Relaxation. The CSA-DD CCR is a NMR phenomenon resulting from the interference of the CSA and dipole–dipole (DD) relaxation mechanisms.^{28,29} The CSA–DD CCR rates depend on mutual orientation of the CSA and DD interaction tensors and thus also on local molecular geometry. The so-called “remote” CSA–DD CCRs, which correlate CSA and DD interactions centered on different nuclei, were previously applied for determination of torsion angles in peptides^{30,31} and NAs.^{8,9,32,33} Theoretical studies provided nonempirical insights into the geometry dependence of the CSA–DD CCR rates, including the effect of geometry dependence of the chemical shielding tensor.^{34,35}

In this work, we focused on the remote CSA–DD cross-correlation between the ^{31}P chemical shielding tensor and the adjacent $\text{C}5'$ – $\text{H}5'$ dipolar vectors. According to the Redfield theory of relaxations, assuming invariable relative orientation of the CSA and DD principal axis frames, the remote transversal CSA–DD CCR rate $\Gamma_{\text{P},\text{CH}}$ is given by^{28,29}

$$\Gamma_{\text{P},\text{CH}} = \frac{1}{2} \frac{\mu_0}{4\pi} \hbar \gamma_{\text{P}} B_0 \frac{\gamma_{\text{C}} \gamma_{\text{H}}}{r_{\text{CH}}^3} \Delta\sigma_{\text{P},\text{CH}}^{\text{eff}} \cdot \frac{4}{3} J(0) \quad (4)$$

where μ_0 is the vacuum permeability, \hbar is the reduced Planck constant, γ_{P} , γ_{C} , and γ_{H} are the gyromagnetic ratios of the ^{31}P , ^{13}C , and ^1H nuclei, B_0 is the magnetic field strength, r_{CH} is the length of the C–H dipolar vector \mathbf{r}_{CH} , $J(0)$ is the spectral density function at zero frequency, and

$$\Delta\sigma_{\text{P},\text{CH}}^{\text{eff}} = \sum_{i=1}^3 \sigma_{\text{P},ii} \frac{3 \cos^2 \theta_{\text{CH},ii} - 1}{2} \quad (5)$$

is the effective CSA, which can be conveniently evaluated by quantum-chemistry methods. Here, $\sigma_{\text{P},ii}$ is the i th principal component of the ^{31}P chemical shielding tensor and $\theta_{\text{CH},ii}$ is the angle between $\sigma_{\text{P},ii}$ and \mathbf{r}_{CH} . We further assume overall isotropic molecular tumbling, for which $J(0) = 2/5\tau_c$, where τ_c is the rotation correlation time. The value $\tau_c = 2.27$ ns determined experimentally for a RNA 14-mer⁹ and the magnetic field $B_0 = 14.09$ T corresponding to the ^1H resonance frequency 600 MHz were used in our calculations.

It should be noted that the isotropic part of the ^{31}P chemical shielding tensor does not contribute to the effective CSA value, because

$$\sum_{i=1}^3 \frac{3 \cos^2 \theta_{\text{CH},ii} - 1}{2} \equiv 0 \quad (6)$$

for any orientation of the chemical shielding tensor. Therefore, only the relative values of principal components $\sigma_{\text{P},ii}^{\text{r}} = \sigma_{\text{P},ii} - \sigma_{\text{P}}$ are essential in the effective CSA, and they can be used instead of $\sigma_{\text{P},ii}$ for calculating the $\Delta\sigma_{\text{P},\text{CH}}^{\text{eff}}$ according to eq 5.

METHODS

Computational Details. All DFT calculations were performed using the B3LYP functional^{36,37} as implemented in the Gaussian 09 package.³⁸ Water solvent in the DFT calculations was simulated with the polarizable continuum model (PCM).³⁹ The coupled-cluster singles and doubles⁴⁰ (CCSD) calculations of geometry and NMR parameters of DMP and PH_3 molecules were performed with the CFOUR program.⁴¹ The DFT and CCSD geometry optimizations employed the 6-31+G(d) and 6-311++G(d,p) basis sets as obtained from the EMSL basis set exchange web portal, respectively.⁴²

The NMR parameters were calculated at the coupled-perturbed B3LYP and CCSD level. The GIAO method^{43–45} was applied in all ^{31}P chemical shielding calculations. The principal components $\sigma_{\text{P},ii}$ and the corresponding eigenvectors were obtained by diagonalizing the symmetric part of the calculated ^{31}P chemical shielding tensor. The Fermi contact (FC), spin–dipolar (SD), paramagnetic spin–orbit (PSO), and diamagnetic spin–orbit (DSO) terms of the total J -coupling were evaluated at the B3LYP level.^{46,47} The FC term of the $^2J_{\text{P},\text{C}}$ coupling was calculated also with the CCSD method. The triplet instability problem⁴⁸ was avoided by applying the orbital-unrelaxed approach in the coupled-cluster calculations (keyword DIFF_TYPE = UNRELAXED). All NMR calculations utilized the IGLO-III basis set; this choice was inspired by our previous work, where the IGLO-III basis provided both ^{31}P chemical shielding and $^2J_{\text{P},\text{C}}$ coupling close to the B3LYP basis-set limit.¹²

Conformational dependencies of the $\Gamma_{\text{P},\text{CH}}$ CCR rates in the EMP molecule were evaluated with two different approaches: (a) both the ^{31}P chemical shielding tensor variation and the molecular geometry relaxation were included in the $\Gamma_{\text{P},\text{CH}}$ calculations (“relaxed approach”); (b) the rigid tensor approximation was adopted, using the ^{31}P chemical shielding tensor calculated in the EMP global minimum ($g-, g-$) and transferring it on rigidly rotated EMP conformers (“rigid approach”).

Molecular Models. We used three different molecular models of NA phosphate. The DMP molecule was employed to compare the performance of the B3LYP and CCSD computational methods. Dependence of NMR parameters on the NA phosphate (ζ , α) conformation was calculated for the EMP molecule (Figure 1b) and the abasic RNA dinucleotide (nPn, Figure 1a), where the NA bases were replaced by methyl groups.

The EMP molecule is the smallest NA phosphate model respecting the asymmetry of the NA backbone. Its conformation is described with torsion angles ζ , α , and β (Figure 1). The global energy minimum with conformation $(\zeta, \alpha, \beta) = (g-, g-, t)$ was optimized at the B3LYP level. The conformational space of EMP was explored by varying the torsion angles ζ and α with 20° steps, resulting in $18 \times 18 = 324$ geometries, while the torsion β was fixed to 180° . The constraint on torsion β reduced the complexity of the problem, and it is consistent with the most usual value of torsion β in NAs.^{1,2} Furthermore, we adopted the (ζ, α, β) values corresponding to the 46 RNA conformational classes found

Table 1. Selected Geometry Parameters^a of NA Phosphate Models

model	geometry method	ζ	α	β	O3'-P-OS'	OP1-P-OP2	P-OP ^b	P-O3'	P-OS'	O3'-C3'	OS'-CS'
DMP	B3LYP	286	286		99.5	125.5	1.504	1.683	1.683	1.418	1.418
DMP	B3LYP/PCM	293	293		102.3	121.7	1.512	1.655	1.655	1.435	1.435
DMP	CCSD	288	288		99.2	125.7	1.488	1.663	1.663	1.412	1.412
EMP	B3LYP/PCM	293	292	180	102.4	121.6	1.512	1.655	1.653	1.434	1.442
nPn1 ^c	Amber99	56	164	152	102.0	120.7	1.471	1.599	1.611	1.416	1.420
nPn2 ^c	"	286	162	163	101.7	121.1	1.473	1.594	1.603	1.414	1.420
nPn3 ^c	"	205	296	153	103.5	121.3	1.474	1.594	1.599	1.417	1.412
nPn6 ^c	"	163	293	167	99.9	121.4	1.473	1.584	1.596	1.411	1.419
nPn9 ^c	"	83	74	172	101.1	120.5	1.473	1.590	1.602	1.414	1.416
nPn12 ^c	"	165	289	166	102.0	121.4	1.472	1.590	1.600	1.414	1.416
nPn15 ^c	"	210	69	195	102.1	121.3	1.473	1.592	1.596	1.413	1.414
nPn18 ^c	"	260	63	179	102.2	120.2	1.474	1.606	1.608	1.417	1.415
nPn20 ^c	"	285	294	179	103.0	120.9	1.473	1.599	1.603	1.416	1.415
DMP ^d	MP2	70	70		99	126	1.51	1.68	1.68	1.43	1.43
BDEP ^e	Exp.	72	68	184 ^f	103.5	121.7	1.513	1.620	1.593	1.474	1.442

^aTorsion and bond angles in deg, bond lengths in Å. ^bAverage P-OP_n bond length, $n = 1, 2$, calculated as P-OP = (P-OP1 + P-OP2)/2. ^cAbasic RNA dinucleotide.⁷ ^dObtained previously by Florián et al. with the 6-31G(d,p) basis set.⁴⁹ ^eX-ray geometry of the barium diethyl phosphate (CSD ID BADET).⁵⁰ Differences in O-P-O-C torsions (ζ and α) and P-O and C-O bond lengths in the structurally symmetric BDEP molecule were caused by crystal packing. ^fAverage value of the P-O-C-C torsion in the BDEP crystal.

Table 2. Isotropic ³¹P Chemical Shifts^a in ppm and ²J_{P,C} Coupling Constants in Hz Calculated with Different Methods and the IGLO-III Basis Set for the (g-, g-) and (t, t) Conformers of DMP

geometry method	NMR method	δ_p^a (g-, g-)/(t, t)	$^{2}J_{P,C}^{FC}$ (g-, g-)/(t, t)	$\Delta_{tt-gg}(\delta_p)$	$\Delta_{tt-gg}(^{2}J_{P,C}^{FC})$
B3LYP	B3LYP	5.2/13.9 ^b	-7.6/-2.1	8.6	5.5
B3LYP/PCM	B3LYP/PCM	8.9/15.3 ^b	-7.5/-2.9	6.5	4.6
CCSD	B3LYP	-0.7/8.2 ^c	-6.8/-1.8	8.9	5.1
CCSD	CCSD	-4.2/4.3 ^d	-6.4/-2.2	8.6	4.2

^aRelative to 85% H₃PO₄ (aq), using the PH₃ secondary standard as described in the Theory section. The calculated values of the ³¹P shielding in PH₃ were: ^b $\sigma_{PH_3} = 566.0$ ppm, ^c $\sigma_{PH_3} = 568.0$ ppm, ^d $\sigma_{PH_3} = 608.4$ ppm.

by Richardson et al.¹ For each (ζ , α , β) geometry of EMP, all remaining coordinates were fully relaxed by B3LYP energy minimization. By optimizing the EMP geometries in this way, we obtained adiabatically relaxed phosphate group geometries, namely, the P-O bond distances and O-P-O valence angles, which most significantly influence the ³¹P NMR parameters in NA phosphate.¹¹

Nine different conformations of nPn (Table 1) were adopted from our previous work.⁷ These structures—further denoted nPn1, nPn2, nPn3, nPn6, nPn9, nPn12, nPn15, nPn18, and nPn20—represent RNA conformational classes 1, 2, 3, 6, 9, 12, 15, 18, and 20 (canonical A-form) as defined by Schneider et al.² The geometries were obtained previously with the Amber99 force field and were used in this work as starting structures for rigid variation of either ζ or α torsion angle, thus sampling the important regions of the (ζ , α) conformational space.

The effects of water solvent on both molecular geometries and NMR parameters were simulated solely with the PCM. Explicit hydration was not applied to avoid steric clashes when sampling the complete (ζ , α) conformational space. The PCM is known to provide only a rough approximation of water solvent effects in NA phosphate.¹² However, absolute accuracy of NMR calculations was not crucial in our case, since we were mainly interested in differences of NMR parameters between different phosphate conformations (“conformational differences”). In this sense, PCM performed rather well and allowed for consistent treatment of water solvent effects in all NA phosphate models used.

For brevity, we used a notation $\Delta_{\zeta'\alpha'-\zeta\alpha}(X)$ standing for the difference of NMR parameter X between (ζ' , α') and (ζ , α) conformers of NA phosphate. For example, the difference of δ_p between the B_{II} and B_I conformers of DNA (“B_{II} – B_I” difference) is denoted $\Delta_{tg-gg}(\delta_p)$.

RESULTS AND DISCUSSION

Geometry Parameters of NA Phosphate Models. The geometries of phosphate group in DMP molecule optimized with the B3LYP and CCSD methods were rather similar, differing only in the P-O bond lengths (Table 1). The gas-phase optimized structures agreed with the DMP geometry obtained previously by Florián et al. at the MP2 level.⁴⁹ The inclusion of water solvent modeled with PCM had a sizable effect on the DMP geometry; the influence of solvent on the NMR (and other) properties of NA phosphate thus originates also from geometry changes.

Molecular geometries optimized with the B3LYP/PCM and Amber99 methods differed (Table 1), which had a sizable effect on the calculated NMR parameters (see below). The geometry of the EMP global minimum (g-, g-) could be directly compared with the nPn20 structure corresponding to the A-form of NAs. Torsion angles α and β obtained in EMP at the B3LYP/PCM level were in very good agreement with the nPn20 force-field values and also with the averaged crystallographic data for the A-form $\alpha = 295^\circ$, $\beta = 174^\circ$.^{1,2} The slight discrepancy in torsion ζ could be attributed to the fact that the C3' methyl group in EMP is a poor substitute for a ribose ring. This limitation of the EMP model was also reflected in the

calculated $^2J_{P,C3'}$ couplings (see below). Bond angles optimized with B3LYP/PCM and Amber99 methods also nicely agreed, but the bond lengths differed, especially for P–OP_n, $n = 1, 2$ (by ~ 0.04 Å) and P–Om', $m = 3, 5$ (by ~ 0.05 Å). This fact has serious consequences for force-field modeling of NA phosphate properties, some of which have been recently addressed.¹²

Benchmark NMR Calculations. We tested the performance of the B3LYP and B3LYP/PCM methods in calculations of the ^{31}P chemical shift δ_{P} and the FC term of the $^2J_{P,C}$ spin–spin coupling against the benchmark CCSD method. The global minimum ($g-, g-$) and transition state (t, t) of the DMP molecule were used for this purpose.

The δ_{P} was quite sensitive to various conditions such as the molecular geometry, the PCM solvation, and the electronic structure method used in the NMR calculations (Table 2). Namely, the calculated δ_{P} values decreased by 5.7–6.0 ppm when the molecular geometries were optimized with the CCSD method instead of B3LYP and by an additional 3.5–3.9 ppm when both structure and NMR shielding were obtained at the CCSD level. The inclusion of PCM solvation, that is currently available only for DFT, led to an increase of δ_{P} by 1.4–3.7 ppm.

The $\Delta_{tt-gg}(\delta_{\text{P}})$ conformational differences of 8.6–8.9 ppm were to a large extent independent of the electronic structure method, indicating that the B3LYP method is well-suited for theoretical modeling of conformational variation of δ_{P} in NA phosphate. The decrease of $\Delta_{tt-gg}(\delta_{\text{P}})$ by ~ 2 ppm induced by the PCM hydration implies that the effect of water solvent on δ_{P} is not uniform but varies with the DMP conformation. Hence, both the DMP polarization and accessibility of the phosphate group by water solvent must be considered for accurate δ_{P} calculations.

The FC term of the $^2J_{P,C}$ coupling is dominant.⁷ The sum of the remaining SD, PSO, and DSO terms ranged from –0.4 to –0.6 Hz for different computational methods and DMP conformers. The J-coupling difference $\Delta_{tt-gg}(^2J_{P,C}^{\text{FC}})$ was overestimated by the B3LYP method relative to CCSD by 1.3 Hz, mainly due to the different performance of B3LYP and CCSD for the ($g-, g-$) conformer (Table 2). The accuracy of the $^2J_{P,C}$ coupling calculated at the B3LYP level therefore varied with the NA phosphate conformation. This fact was taken into account when estimating the accuracy of the calculated structural dependencies of $^2J_{P,C}$ couplings. Other DFT functionals performed similarly as the B3LYP; the $^2J_{P,C}^{\text{FC}}$ values for the ($g-, g-$) conformer of DMP calculated with BLYP, BPW91, and B3PW91 functionals were 7.3, 7.2, and 7.4 Hz.

We also compared the performance of the B3LYP, B3LYP/PCM, and CCSD methods in calculations of the full ^{31}P chemical shielding tensor (Supporting Information, Table S1). The principal components $\sigma_{P,ii}$, $ii = 11, 22, 33$, calculated with the CCSD method differed by 6–14 ppm from those obtained with B3LYP. The inclusion of PCM hydration in the B3LYP calculations had a much larger impact; the $\sigma_{P,ii}$ values changed by 22–50 ppm. The ^{31}P -CSA calculated at the CCSD level was by 21 ppm smaller than that obtained using B3LYP. The inclusion of PCM hydration decreased the ^{31}P -CSA by more than 60 ppm. The principal components $\sigma_{P,ii}$ were thus much more sensitive to the NMR computational method and water solvent description than the isotropic chemical shift δ_{P} itself. Interestingly, the orientation of the ^{31}P chemical shielding tensor in the phosphate–frame coordinate system²⁰ represented by angles φ_{ii} , $ii = 11, 22, 33$ (Figure 2), was practically independent of the computational method.

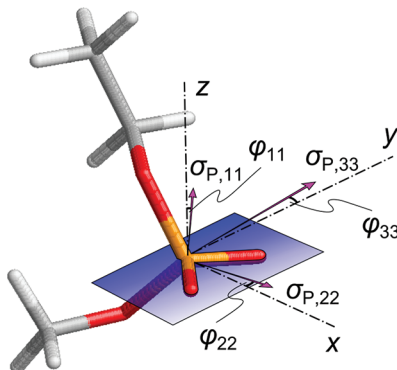


Figure 2. Schematic representation of the ^{31}P chemical shielding tensor in the EMP molecule: principal components $\sigma_{P,ii}$ and their orientations φ_{ii} , $ii = 11, 22, 33$, in the phosphate–frame coordinate system.²⁰

Our results are consistent with previous calculations by Přečeková et al., who found that the ^{31}P -CSA values calculated in DMP with two explicit hydration patterns were by up to 130 ppm smaller than the ^{31}P -CSA in the gas phase.¹⁵ The PCM hydration thus accounted for approximately half of the effect of static hydration on ^{31}P -CSA and also on principal components $\sigma_{P,ii}$ (Supporting Information, Table S1). We note that neither implicit PCM nor static hydration can be regarded as a correct description of phosphate solvation. According to the current state of knowledge, dynamical averaging of explicit solvent is probably the best theoretical method for modeling the solvation effects on NMR parameters in NA phosphate.^{12,14}

The benchmark NMR calculations showed that the B3LYP method performs rather well for both ^{31}P chemical shift and $^2J_{P,C}$ coupling. We found that hydration has a larger impact on the calculated NMR parameters than the particular choice of electronic structure method. Solvation effects should be therefore always included in NMR calculations in NA phosphate.

Geometry Dependence of ^{31}P Chemical Shift. The δ_{P} calculated in the EMP molecule ranged from 0.7 ppm for the rather unrealistic ($0^\circ, 0^\circ$) phosphate conformer to 13.8 ppm for the (t, t) conformer (Figure 3). The δ_{P} values of ~ 7.5 –8.0 ppm calculated for the ($g-, g-$) region dominantly populated in NAs were somewhat larger than the values of –2.0–0.5 ppm typically measured in NAs.^{10,11} This difference can be attributed to intrinsic errors of the DFT chemical shielding calculations, to insufficient accounting for water solvent by PCM, and to improperly described ^{31}P NMR reference via the secondary standard approach. However, these systematic computational errors tend to mutually cancel when calculating the chemical shift differences between different conformers (see Table 2). Hence, the geometry trends calculated for δ_{P} can be trusted more than the absolute δ_{P} values.

The δ_{P} values calculated for the nPn structures were by ~ 25 ppm smaller than those obtained for the corresponding (ζ, α) conformers of EMP (Supporting Information, Figure S1). This difference originates from the differences in local phosphate geometry optimized with the Amber99 and B3LYP methods (Table 1). Interestingly, the dependencies of δ_{P} on the (ζ, α) conformation calculated for both EMP and nPn possessed a very similar shape, thus indicating that a qualitatively correct geometry dependence of δ_{P} can be obtained even with the smaller EMP model.

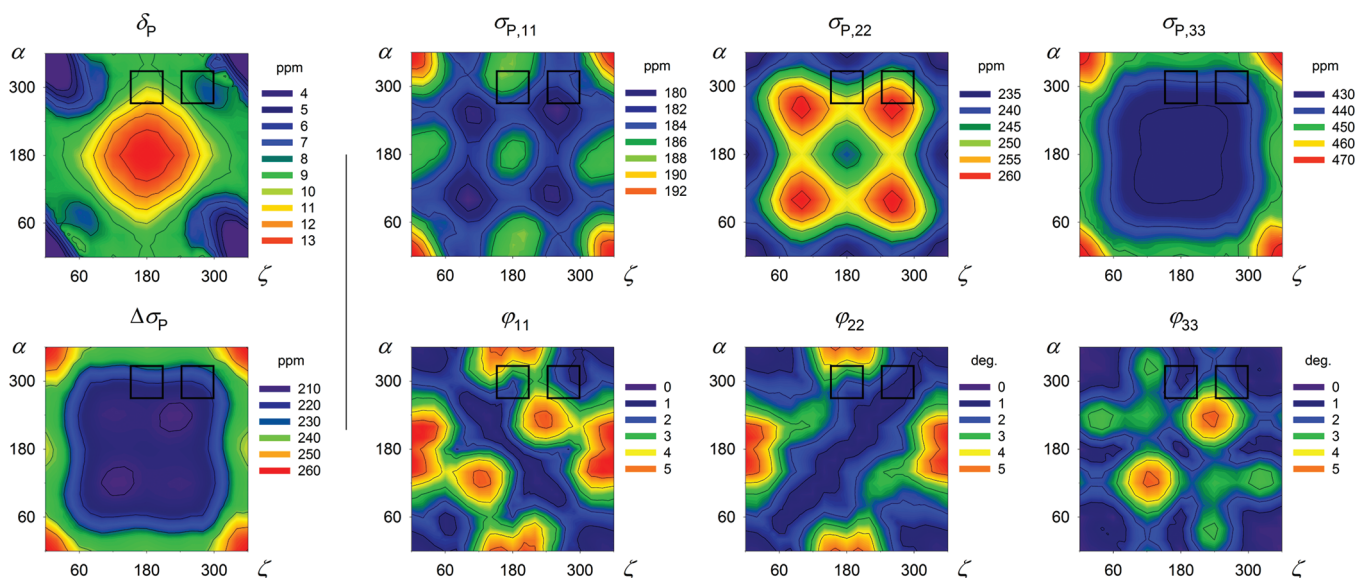


Figure 3. Dependencies of isotropic ^{31}P chemical shift δ_{P} , chemical shielding anisotropy $\Delta\sigma_{\text{P}}$, principal components $\sigma_{\text{P},ii}$ of the ^{31}P chemical shielding tensor and their orientations in the molecular frame φ_{ii} , $ii = 11, 22, 33$, on the (ζ, α) conformation of the EMP molecule calculated with the B3LYP/PCM method. Black squares indicate the (ζ, α) regions that were explored previously by Přečeková et al.¹⁵

Table 3. Comparison of the $B_{\text{II}} - B_{\text{I}}$ Differences of δ_{P} in ppm, Principal Components $\sigma_{\text{P},ii}$ in ppm, $ii = 11, 22, 33$, and $^2J_{\text{P},\text{C}3'}$ Coupling in Hz, Obtained with Different Computational Approaches

model	geometry method	NMR method	$\Delta_{\text{tg-gg}}$				
			δ_{P}	$\sigma_{\text{P},11}$	$\sigma_{\text{P},22}$	$\sigma_{\text{P},33}$	$^2J_{\text{P},\text{C}3'}$
EMP ^a	B3LYP	B3LYP	3.8	6.9	4.3	-11.2	3.3
EMP-PCM ^a	B3LYP/PCM	B3LYP/PCM	2.3	4.0	-0.4	-3.6	2.2
nPn ^b	Amber99	B3LYP/PCM	1.8, 1.9, 2.6				2.2, 2.2, 2.3
DMP ^{a,c}	B3LYP	SOS-DFPT-IGLO-PWP86	6.9	8.8	2.5	-11.3	
DMP-IC ^{a,c}	"	"	5.9	8.5	-2.2	-6.4	
DMP-SC ^{a,c}	"	"	3.8	7.9	1.2	-8.9	
B-DNA ^d	Amber99	"	2.1, 1.6				
B-DNA ^e	Exp.	Exp.	1.6				

^aCalculated as differences between the $(180^\circ, 300^\circ)$ and $(300^\circ, 300^\circ)$ conformers. ^bResults obtained as differences between the respective conformers of nPn3, nPn12, and nPn20. ^cReference 15; IC and SC denote two different explicit hydration patterns. ^dReference 14; results for two phosphate residues of a Dickerson–Drew DNA dodecamer obtained by averaging of the respective δ_{P} values over MD trajectory. ^eReference 10.

Conformational differences of δ_{P} were in good agreement with available experimental and theoretical data. The B3LYP/PCM calculations satisfactorily reproduced the ^{31}P chemical shift difference between the B_{I} and B_{II} conformations of the NA backbone (Table 3). Relative chemical shifts $\Delta_{\text{tg-gg}}(\delta_{\text{P}})$ calculated in EMP (2.3 ppm) and nPn (1.8, 1.9, and 2.6 ppm) nicely coincided with the experimental $B_{\text{II}} - B_{\text{I}}$ difference¹⁰ (1.6 ppm). Previous theoretical calculations of $\Delta_{\text{tg-gg}}(\delta_{\text{P}})$ in DMP with two different explicit hydration patterns provided somewhat dispersed values (5.9 and 3.8 ppm, Table 3),¹⁵ which anticipated the need of dynamic averaging of explicit hydration surrounding phosphate to obtain converged results (2.1, 1.6 ppm).¹⁴ The need of dynamic averaging of explicit solvent was also concluded in calculations of solvation effects on ^{31}P NMR parameters in NA phosphate.¹² However, in the case of a large number of conformations like here, the dynamic approach becomes rather costly and implicit solvation may be the only feasible option. The PCM actually performed rather well, because it accounted for a large part of the conformation-dependent water solvent effect on the ^{31}P chemical shift: the $\Delta_{\text{tg-gg}}(\delta_{\text{P}})$ calculated in the gas phase was 3.8 ppm, with PCM it was 2.3 ppm, and the experimental value is

1.6 ppm. The comparison of calculated $\Delta_{\text{tg-gg}}(\delta_{\text{P}})$ values with the experimentally known $B_{\text{II}} - B_{\text{I}}$ difference thus indicates that conformational differences of δ_{P} calculated with the B3LYP/PCM method are qualitatively correct.

To the best of our knowledge, the theoretical δ_{P} data available in the literature were calculated either for a limited set of (ζ, α) phosphate conformations^{15,18} or for full variation of torsion angles ζ and α with a crude semiempirical approach.⁵¹ Our DFT calculations provide consistent theoretical insight into the complete dependence of δ_{P} on the (ζ, α) conformation of NA phosphate.

Geometry Dependences of ^{31}P Chemical Shielding Tensor Components. Variation of principal components $\sigma_{\text{P},ii}$, $ii = 11, 22, 33$, by up to 15, 31, and 46 ppm, respectively (Figure 3), calculated with the B3LYP/PCM method was much larger than the range of isotropic values δ_{P} (\sim 13 ppm). This could be explained by mutual compensation of the components. Namely, the $\sigma_{\text{P},11}$ and $\sigma_{\text{P},22}$ surfaces were nearly complementary, implying that the geometry dependencies of both δ_{P} and $\Delta\sigma_{\text{P}}$ are to a large extent dominated by the $\sigma_{\text{P},33}$ component (Figure 3).

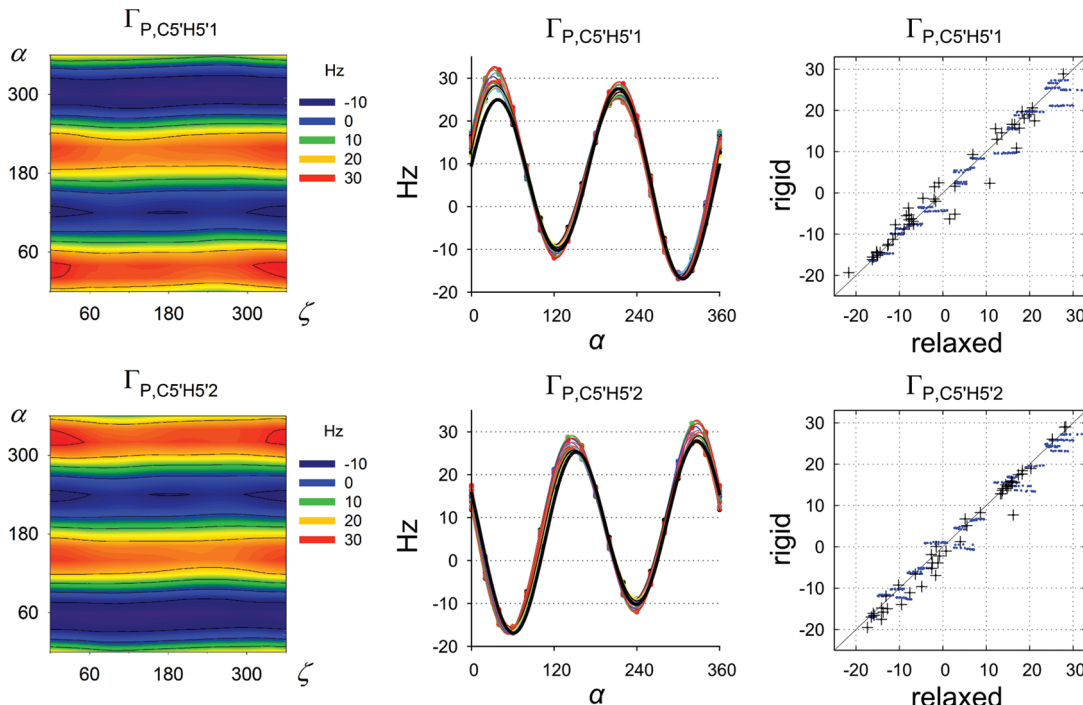


Figure 4. (left) Dependencies of the $\Gamma_{P,C5'H5'}$ and $\Gamma_{P,C5'H5'}$ cross-correlated relaxation rates on the (ζ, α) conformation of EMP calculated using the “relaxed” approach. (middle) Comparison of the “rigid” (thick black line) and “relaxed” approach (colored lines; each line corresponds to a specific value of torsion ζ ranging from 0 to 340°), here displayed in dependence on torsion α only. (right) Correlation between the “rigid” and “relaxed” approach in the calculations of $\Gamma_{P,C5'H5'}$ and $\Gamma_{P,C5'H5'}$ (in Hz) for EMP grid-point geometries with $\beta = 180^\circ$ (blue dots) and for EMP geometries sampling the RNA structural classes (black crosses).

The geometry dependences of principal components of the ^{31}P chemical shift tensor $\delta_{P,ii}$ calculated with the secondary standard approach (eq 2) were in qualitative agreement with previously calculated data for explicitly hydrated DMP in $(t, g-)$ and $(g-, g-)$ conformations¹⁵ (Supporting Information, Figure S3). In the two conformational regions, the principal component $\delta_{P,22}$ consistently increased and $\delta_{P,33}$ decreased with the increase of torsion α . The $\delta_{P,ii}$ values, $ii = 22, 33$, calculated in this work varied in the $(t, g-)$ and $(g-, g-)$ regions by ca. 15–20 ppm, which is significantly less than calculated previously in explicitly hydrated DMP¹⁵ (by ca. 25–30 ppm). Variation of the $\delta_{P,11}$ component was only a few ppm both in this and previous work. The isotropic δ_p values consistently decreased with increasing torsion α . The decrease, which was larger in the $(t, g-)$ region, was more pronounced in the previous work by Precechtělová et al. than in this work, which was probably caused by the difference between explicit and implicit phosphate hydration. Interestingly, our calculations provided quite similar $B_{II} - B_I$ differences of $\sigma_{P,ii}$ as obtained previously for the explicitly hydrated DMP–IC model¹⁵ (Table 3).

The orientation of the ^{31}P chemical shielding tensor in the phosphate–frame coordinate system was nearly independent of the EMP conformation because the calculated angles φ_{ii} were smaller than 6° (Figure 3). This agrees with the previous theoretical results¹⁵ but conflicts with the experimental solid-state NMR data for a crystal of BDEP ($\varphi_{11} = 7^\circ$, $\varphi_{22} = 13^\circ$, $\varphi_{33} = 9^\circ$).²⁰ We have to keep in mind that the first coordination shell of the phosphate group in the BDEP crystal structure contains only Ba^{2+} ions.⁵⁰ In our previous work, we showed that direct coordination of divalent ion to the phosphate group has a significant impact on the ^{31}P chemical shielding tensor.¹²

Therefore, we propose that the ^{31}P shielding tensor measured in the BDEP crystal was influenced by direct coordination of Ba^{2+} ions and that the φ_{ii} values smaller than 6° are natural for all (ζ, α) conformations of NA phosphate.

$\Gamma_{P,C5'H5'}$ Cross-Correlated Relaxation Rates. We showed above that the principal components $\sigma_{P,ii}$ vary significantly with rotation of torsion angles ζ and α , by up to 46 ppm (Figure 3). The question is to what extent this behavior affects the $\Gamma_{P,\text{CH}}$ CCR rates and how large could be the error when applying the rigid tensor approximation. We could answer this question by calculating the $\Gamma_{P,C5'H5'}$ and $\Gamma_{P,C5'H5'}$ CCR rates in EMP with the “relaxed” and “rigid” approach described in the Methods section.

The $\Gamma_{P,C5'H5'}$ and $\Gamma_{P,C5'H5'}$ CCR rates depend dominantly on torsion angles α and β .^{8,9} The EMP calculations with $\beta = 180^\circ$ show only the dependence on torsions ζ and α (Figure 4, left). To see the effect of β variation, we calculated the CCR rates also for the EMP geometries sampling the RNA structural classes,¹ where the torsion β varies from 83 to 248° (Supporting Information, Figure S2).

The CCR rates obtained with the “rigid” approach are inherently independent of torsion angle ζ . The application of the “relaxed” approach only slightly perturbed the one-dimensional character of the two dependencies (Figure 4, middle). Both $\Gamma_{P,C5'H5'}$ and $\Gamma_{P,C5'H5'}$ ranged from ca. –17 to 32 Hz. The difference between CCR rates calculated using the “rigid” and “relaxed” approach was on average over all EMP geometries smaller than 2 Hz. By detailed analysis of the calculated data (not shown), we found that the differences were caused by both conformational variation of the ^{31}P chemical shielding tensor and geometry relaxation of the C5’–H5’ bond vectors affecting the angles $\vartheta_{\text{CH},ii}$ in eq 5. The r_{CH}^{-3} factor varied by 1.6% at most; its influence on the CCR rates was thus

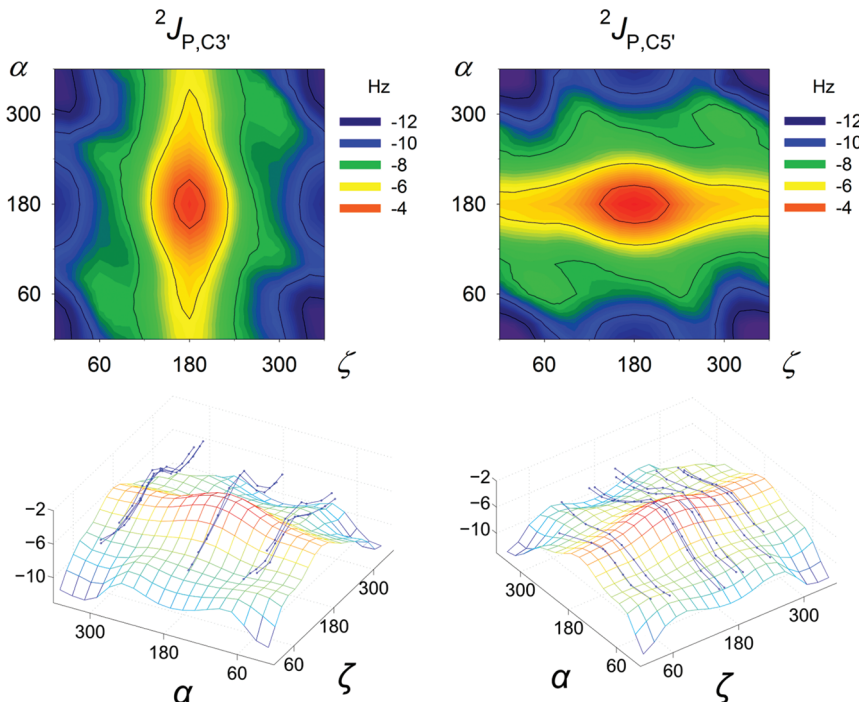


Figure 5. (top) Dependencies of the $^2J_{P,C3'}$ and $^2J_{P,C5'}$ coupling constants in Hz on the (ζ, α) conformation of EMP. (bottom) Comparison of $^2J_{P,C}$ couplings calculated in EMP (colored surfaces; the grid represents the calculated data points) and nPn (blue lines; dots mark the calculated data points) molecules.

negligible. The rigid tensor approximation can be therefore considered valid for the $\Gamma_{P,CH}$ CCR rates in NA phosphate.

$^2J_{P,C}$ Coupling Constants. For the first time, the dependencies of $^2J_{P,C3'}$ and $^2J_{P,C}$ coupling constants on the (ζ, α) conformation of NA phosphate are reported (Figure 5). We obtained two coherent sets of theoretical data for EMP and nPn molecules. While the EMP calculations sample the complete (ζ, α) dependence of the two J -couplings, the nPn data were obtained for selected NA backbone classes by stepwise variation of one of the two torsion angles. The $^2J_{P,C5'}$ coupling depends dominantly on torsion angle α and the $^2J_{P,C3'}$ coupling on torsion ζ , but the dependence on the second P–O torsion is also not negligible. The two-dimensional dependencies of $^2J_{P,C3'}$ and $^2J_{P,C5'}$ are similar owing to the symmetry of NA phosphate. The $^2J_{P,C}$ couplings are negative for all phosphate conformations. For better clarity, and also because the sign of the $^2J_{P,C}$ coupling is usually not determined experimentally, we further discuss only the absolute $^2J_{P,C}$ values.

The two $^2J_{P,C}$ couplings calculated in the EMP molecule range approximately from 3 to 13 Hz (Figure 5). Some conformers of NA phosphate can be clearly distinguished with the $^2J_{P,C}$ couplings. The lowest values near 3 Hz were obtained for the (t, t) conformer, while the values corresponding to the most populated NA conformer ($g-, g-$) were around 8 Hz. Unfortunately, the $g+$ and $g-$ conformation of both ζ and α torsion angles are hardly distinguishable, since they both correspond to similar values of $^2J_{P,C}$. The $B_I \rightarrow B_{II}$ transition calculated as a change of the (ζ, α) conformation from $(g-, g-)$ to $(t, g-)$ was accompanied by ~ 2 – 3 Hz decrease of the $^2J_{P,C3'}$ coupling (Table 3, Figure 5), which is in agreement with our previous work for NA conformational classes.⁷ Similarly, the transition of torsion α from *gauche* to *trans* corresponds to a significant decrease of $^2J_{P,C5'}$. Also, the effect of neighboring torsions ε and β may not be negligible. For example, the $^2J_{P,C5'}$

coupling notably increases when β exceeds the 120 – 240° interval (Supporting Information, Figure S5).

Experimentally, the $^2J_{P,C}$ couplings typically occur between 1 and 6.5 Hz.²¹–²⁵ Structural interpretation of the measured values in terms of torsions ζ and α was so far unavailable. Here, we correlated the experimental $^2J_{P,C}$ couplings with torsion angles ζ and α for NA molecules with known structures: cyclic d dinucleotide,²¹ 10 base-pair (bp) long DNA duplex oligonucleotide^{23,52} (PDB ID 1NEV), and 8 bp long stem of hairpin-35 of 23S rRNA²⁵ (PDB ID 2GBH). The NMR data for the most populated NA conformer ($g-, g-$) were used to validate our theoretical approach. The experimental $^2J_{P,C}$ couplings for the $(g-, g-)$ conformer ranged from 4.5 to 5.5 Hz (Supporting Information, Table S2 and Figure S4), while the values calculated in EMP were near 8 Hz (Table 4). The deviation from experiment can be explained by imperfections of the B3LYP method in both geometry and NMR calculations, the effect of incomplete basis set, and the error of PCM in describing the phosphate hydration (Table 4). The dynamically averaged effect of solvent on $^2J_{P,C}$ values would be even larger when considering NA phosphate solvation with metal cation, as was reported in our previous work.¹² Somewhat larger deviations of the calculated $^2J_{P,C}$ values from experiment were obtained for other phosphate conformations; similar sources of computational errors can be expected, but their values are not known. Nevertheless, we can anticipate that the geometry dependencies of the $^2J_{P,C}$ couplings calculated with the B3LYP/PCM method are qualitatively correct, albeit the $^2J_{P,C}$ magnitudes are overestimated.

The nPn calculations provide an important link between the simple EMP model and actual NA backbone structure. The $^2J_{P,C}$ couplings calculated in the EMP and nPn molecules for the same (ζ, α) conformers differ (Figure 5), mainly due to different local geometries of NA phosphate (Table 1) and also

Table 4. Comparison of the Calculated $^2J_{P,C}$ Coupling Values and Corrections ΔJ (in Hz) with Available Experimental Data for the Most Populated Phosphate Conformer ($g-, g-$)

J-coupling contributions	$^2J_{P,C3'}$	$^2J_{P,CS'}$
J : B3LYP/PCM ^a	-8.1	-7.7
ΔJ : geometry ^b	+0.7	
ΔJ : electron correlation ^c	+0.5	
ΔJ : basis set ^d	+0.5	
ΔJ : explicit solvent ^e	+0.9	-0.5
J : total	-5.4	-6.6
$ J $: experiment ^f	4.5–5.5	

^aCalculated for the ($\zeta = 280^\circ$, $\alpha = 300^\circ$, $\beta = 180^\circ$) conformer of EMP, using the IGLO-III basis set. ^bThe effect of molecular geometry obtained as a difference between the $^2J_{P,C}$ values calculated for DMP optimized with the CCSD and B3LYP methods (Table 2). ^cThe effect of the NMR calculation method obtained as a difference between the $^2J_{P,C}^{FC}$ values calculated in DMP with the CCSD and B3LYP methods (Table 2). ^dThe effect of basis set obtained as a difference between $^2J_{P,C}$ values calculated in EMP with the B3LYP/aug-cc-pCVQZ (near basis-set limit) and B3LYP/IGLO-III methods.¹² ^eThe effect of dynamically averaged explicit solvent obtained as a difference between the $^2J_{P,C}$ values calculated for A-RNA dinucleotide with dynamically averaged explicit water solvent (-6.9 and -6.8 Hz with the uncertainty of ~0.4 Hz; see our previous work¹²) and the respective values calculated here for the same model with the same computational method employing PCM of water solvent (-7.9 and -6.3 Hz). ^fThe experimental $^2J_{P,C}$ couplings for the ($g-, g-$) conformer taken from refs 23 and 25 (see also the Supporting Information, Table S2 and Figure S4).

because of the improper termination of the EMP molecule at C3' carbon. On the other hand, the dependencies obtained with the two NA phosphate models correspond qualitatively to each other, showing the same conformational trends (Figure 5). The $^2J_{P,C3'}$ and $^2J_{P,CS'}$ couplings calculated for the ($g-, g-$) conformer of nPn ranged from 4.9 to 6.3 Hz and from 6.7 to 7.5 Hz, respectively. The J -couplings calculated with presumably lower quality force-field geometries were thus closer to the experimental range 4.5–5.5 Hz than those obtained for the DFT-optimized EMP structures. This was probably caused by error cancellation. Nevertheless, the correspondence between geometry trends calculated in EMP and nPn indicates that the dependencies shown in Figure 5 should be generally valid for the NA backbone.

Structural interpretation of the $^2J_{P,C3'}$ and $^2J_{P,CS'}$ couplings can be only qualitative, namely, because the two-dimensional character of their dependences implies that similar $^2J_{P,C}$ values may correspond to different phosphate conformers. Furthermore, the computational imperfections mentioned above and the uncertainty of experimental determination of $^2J_{P,C}$ couplings (which may be larger than 1 Hz^{23,24}) prohibited so far their accurate calibration. Nevertheless, we found that the $^2J_{P,C3'}$ and $^2J_{P,CS'}$ couplings can be loosely assigned to NA backbone torsion angles ζ and α , respectively. On the basis of our calculations and comparison with available experimental data, we propose two qualitative rules: (a) The $^2J_{P,C}$ coupling smaller than ~3 Hz should indicate the orientation of the assigned torsion angle (ζ or α) that is different from typical *gauche* (near 70 or 290°). (b) The $^2J_{P,C}$ coupling larger than ~4.5 Hz should indicate that the orientation of the assigned torsion angle deviates from the 120–240° region. The $^2J_{P,C}$ values between 3 and 4.5 Hz are difficult to interpret in terms of torsions ζ and α because the dominant J -coupling dependence on the assigned

torsion is largely perturbed by variation of the second torsion. These rules may serve as qualitative restraints on phosphate conformation in NMR structural studies of NAs. Their further validation based on more extended comparison with accurate experimental data is clearly advisable.

$^3J_{P,C4'}$ Coupling. The $^3J_{P,C4'}$ coupling is assigned to torsion angle β with a standard Karplus equation.^{22,53,54} The structural interpretation of $^3J_{P,C4'}$ relies on its independence of other torsion angles. To validate this assumption, we calculated the dependence of the $^3J_{P,C4'}$ coupling on torsion angles ζ and α in the EMP molecule. The calculated variation of $^3J_{P,C4'}$ was quite large, ca. 2 Hz (Supporting Information, Figure S6). Such variation in the $^3J_{P,C4'}$ value interpreted with standard Karplus equations can cause error in determination of the assigned torsion β as large as ~25°.

The calculations thus revealed that variation of the NA phosphate conformation may affect the spin–spin coupling pathways between phosphorus and relatively distant atoms. This could have been foreseen, since the complicated electronic structure of negatively charged NA phosphate sensitively responds to the local geometry deformations and a perturbation at one side of the spin–spin coupling pathway is in this way promoted to the total J -coupling value.

CONCLUSIONS

In this theoretical work, the isotropic ^{31}P chemical shift, the principal components $\sigma_{P,ii}$ of the ^{31}P chemical shielding tensor, and their orientations in the molecular frame, the $\Gamma_{P,CS'HS'1}$ and $\Gamma_{P,CS'HS'2}$ cross-correlated relaxation rates, as well as the $^2J_{P,C3'}$, $^2J_{P,CS'}$, and $^3J_{P,C4'}$ coupling constants were calculated in dependence on nucleic acid backbone torsion angles ζ and α .

Although the NMR calculations did not provide absolute accuracy of the isotropic ^{31}P chemical shift, the relative values for different phosphate conformations were in good agreement with previous experimental and theoretical data. Geometry dependencies of both isotropic ^{31}P chemical shift and chemical shielding anisotropy were dominated by the $\sigma_{P,33}$ principal component, owing to mutual compensation of the $\sigma_{P,11}$ and $\sigma_{P,22}$ components. Deviations of the ^{31}P principal components from phosphate frame axes were smaller than 6°. The orientation of the ^{31}P chemical shielding tensor in the molecular frame is thus almost independent of torsion angles ζ and α .

We found that the $\Gamma_{P,CS'HS'1}$ and $\Gamma_{P,CS'HS'2}$ cross-correlated relaxation rates are nearly independent of torsion angle ζ , being only slightly modulated by the conformational variation of the ^{31}P chemical shielding tensor and local phosphate geometry. The approximation assuming a rigid ^{31}P chemical shielding tensor can be thus considered valid for the interpretation of $\Gamma_{P,CH}$ cross-correlated relaxation rates in nucleic acids.

DFT calculations of $^2J_{P,C}$ coupling constants in nucleic acid backbone revealed their strong dependence on both torsion angles ζ and α with dominant modulation by only one of the torsions. The $^2J_{P,C3'}$ and $^2J_{P,CS'}$ couplings thus could be structurally assigned to torsions ζ and α , respectively, and interpreted as loose restraints on the phosphate conformation. The absolute $^2J_{P,C}$ values calculated with the B3LYP/PCM method were overall overestimated relative to the experiment. Computational errors for the most populated phosphate conformer ($g-, g-$) were ascribed to imperfect performance of the DFT method, which was tested against the benchmark CCSD method, incomplete atomic basis set, and incomplete

description of phosphate hydration by PCM. Our results provide the missing link between the $^2J_{P,C3'}$ and $^2J_{P,CS'}$ spin–spin coupling constants and the NA backbone torsion angles ζ and α .

ASSOCIATED CONTENT

Supporting Information

Comparison of the dependencies of ^{31}P chemical shift on the (ζ, α) conformation of EMP and nPn. Correlation between backbone torsion angles ζ , α , and β in RNA conformational classes. Comparison of calculated principal components of the ^{31}P chemical shielding tensor and their orientations in the phosphate–frame coordinate system with previous theoretical results and NMR experiment. Correlation of available experimental $^2J_{P,C}$ couplings with torsion angles ζ and α . Dependence of the $^2J_{P,CS'}$ coupling on torsion angle β . Dependence of the $^3J_{P,C4'}$ coupling on the (ζ, α) conformation of EMP. Optimized geometries of the DMP and EMP models. This material is available free of charge via the Internet at <http://pubs.acs.org>.

AUTHOR INFORMATION

Corresponding Author

*E-mail: ladislav.benda@uochb.cas.cz (L.B.); vladimir.sychrovsky@uochb.cas.cz (V.S.). Phone: +420 220 183 234. Fax: +420 220 183 578.

Notes

The authors declare no competing financial interest.

ACKNOWLEDGMENTS

This work was supported by the Czech Science Foundation, Grant No. 205/10/0228. Z.S.V. and M.S. acknowledge support by the Czech Science Foundation, Grant Nos. P208/10/P398 and 203/09/2037, respectively. V.S. was supported by a Human Frontier Science Program (HFSP) Young Investigator's Grant.

REFERENCES

- Richardson, J. S.; Schneider, B.; Murray, L. W.; Kapral, G. J.; Immormino, R. M.; Headd, J. J.; Richardson, D. C.; Ham, D.; Hershkovits, E.; Williams, L. D.; Keating, K. S.; Pyle, A. M.; Micallef, D.; Westbrook, J.; Berman, H. M. *RNA* **2008**, *14*, 465–481.
- Schneider, B.; Morávek, Z.; Berman, H. M. *Nucleic Acids Res.* **2004**, *32*, 1666–1677.
- Varani, G.; Aboul-ela, F.; Allain, F. H.-T. *Prog. Nucl. Magn. Reson. Spectrosc.* **1996**, *29*, 51–127.
- Wijmenga, S. S.; van Buuren, B. N. M. *Prog. Nucl. Magn. Reson. Spectrosc.* **1998**, *32*, 287–387.
- Fürtig, B.; Richter, C.; Wohner, J.; Schwalbe, H. *ChemBioChem* **2003**, *4*, 936–962.
- Flinders, J.; Dieckmann, T. *Prog. Nucl. Magn. Reson. Spectrosc.* **2006**, *48*, 137–159.
- Sychrovský, V.; Vokáčová, Z.; Šponer, J.; Špacková, N.; Schneider, B. *J. Phys. Chem. B* **2006**, *110*, 22894–22902.
- Richter, C.; Reif, B.; Griesinger, C.; Schwalbe, H. *J. Am. Chem. Soc.* **2000**, *122*, 12728–12731.
- Nozinovic, S.; Richter, C.; Rinnenthal, J.; Fürtig, B.; Duchardt-Ferner, E.; Weigand, J. E.; Schwalbe, H. *J. Am. Chem. Soc.* **2010**, *132*, 10318–10329.
- Gorenstein, D. G. *Chem. Rev.* **1994**, *94*, 1315–1338.
- Gorenstein, D. G. *Phosphorus-31 NMR*; Academic Press: Orlando, FL, 1984.
- Benda, L.; Schneider, B.; Sychrovský, V. *J. Phys. Chem. A* **2011**, *115*, 2385–2395.
- Ribas Prado, F.; Giessner-Prettre, C.; Pullman, B.; Daudey, J. P. *J. Am. Chem. Soc.* **1979**, *101*, 1737–1742.
- Přečechtělová, J.; Novák, P.; Munzarová, M. L.; Kaupp, M.; Sklenář, V. *J. Am. Chem. Soc.* **2010**, *132*, 17139–17148.
- Přečechtělová, J.; Munzarová, M. L.; Novák, P.; Sklenář, V. *J. Phys. Chem. B* **2007**, *111*, 2658–2667.
- Gorenstein, D. G. *J. Am. Chem. Soc.* **1975**, *97*, 898–900.
- Giessner-Prettre, C.; Pullman, B.; Parado, F. R.; Cheng, D. M.; Iuorno, V.; Ts' O, P. O. P. *Biopolymers* **1984**, *23*, 377–388.
- Přečechtělová, J.; Padrtá, P.; Munzarová, M. L.; Sklenář, V. *J. Phys. Chem. B* **2008**, *112*, 3470–3478.
- Lerner, D. B.; Becktel, W. J.; Everett, R.; Goodman, M.; Kearns, D. R. *Biopolymers* **1984**, *23*, 2157–2172.
- Herzfeld, J.; Griffin, R. G.; Haberkorn, R. A. *Biochemistry* **1978**, *17*, 2711–2718.
- Blommers, M. J. J.; Haasnoot, C. A. G.; Walters, J.; Vandermarel, G. A.; Vanboom, J. H.; Hilbers, C. W. *Biochemistry* **1988**, *27*, 8361–8369.
- Mooren, M. M. W.; Wijmenga, S. S.; Vandermarel, G. A.; Vanboom, J. H.; Hilbers, C. W. *Nucleic Acids Res.* **1994**, *22*, 2658–2666.
- Zimmer, D. P.; Marino, J. P.; Griesinger, C. *Magn. Reson. Chem.* **1996**, *34*, S177–S186.
- Richter, C.; Reif, B.; Worner, K.; Quant, S.; Marino, J. P.; Engels, J. W.; Griesinger, C.; Schwalbe, H. *J. Biomol. NMR* **1998**, *12*, 223–230.
- O'Neil-Cabello, E.; Wu, Z. R.; Bryce, D. L.; Nikonorowicz, E. P.; Bax, A. *J. Biomol. NMR* **2004**, *30*, 61–70.
- van Wüllen, C. *Phys. Chem. Chem. Phys.* **2000**, *2*, 2137–2144.
- Jameson, C. J.; de Dios, A. C.; Jameson, A. K. *Chem. Phys. Lett.* **1990**, *167*, 575–582.
- Kumar, A.; Grace, R. C. R.; Madhu, P. K. *Prog. Nucl. Magn. Reson. Spectrosc.* **2000**, *37*, 191–319.
- Kowalewski, J.; Mäler, L. *Nuclear Spin Relaxation in Liquids: Theory, Experiments, and Applications*; Taylor & Francis Group: New York, London, 2006.
- Reif, B.; Hennig, M.; Griesinger, C. *Science* **1997**, *276*, 1230–1233.
- Reif, B.; Diener, A.; Hennig, M.; Maurer, M.; Griesinger, C. *J. Magn. Reson.* **2000**, *143*, 45–68.
- Duchardt, E.; Richter, C.; Ohlenschläger, O.; Gorlach, M.; Wohner, J.; Schwalbe, H. *J. Am. Chem. Soc.* **2004**, *126*, 1962–1970.
- Rinnenthal, J.; Richter, C.; Ferner, J.; Duchardt, E.; Schwalbe, H. *J. Biomol. NMR* **2007**, *39*, 17–29.
- Sychrovský, V.; Müller, N.; Schneider, B.; Smrečki, V.; Špirko, V.; Šponer, J.; Trantirek, L. *J. Am. Chem. Soc.* **2005**, *127*, 14663–14667.
- Benda, L.; Bouř, P.; Müller, N.; Sychrovský, V. *J. Phys. Chem. B* **2009**, *113*, 5273–5281.
- Becke, A. D. *J. Chem. Phys.* **1993**, *98*, 5648–5652.
- Lee, C. T.; Yang, W. T.; Parr, R. G. *Phys. Rev. B* **1988**, *37*, 785–789.
- Frisch, M. J.; Trucks, G. W.; Schlegel, H. B.; Scuseria, G. E.; Robb, M. A.; Cheeseman, J. R.; Scalmani, G.; Barone, V.; Mennucci, B.; Petersson, G. A.; Nakatsuji, H.; Caricato, M.; Li, X.; Hratchian, H. P.; Izmaylov, A. F.; Bloino, J.; Zheng, G.; Sonnenberg, J. L.; Hada, M.; Ehara, M.; Toyota, K.; Fukuda, R.; Hasegawa, J.; Ishida, M.; Nakajima, T.; Honda, Y.; Kitao, O.; Nakai, H.; Vreven, T.; Montgomery, J. A., Jr.; Peralta, J. E.; Ogliaro, F.; Bearpark, M.; Heyd, J. J.; Brothers, E.; Kudin, K. N.; Staroverov, V. N.; Kobayashi, R.; Normand, J.; Raghavachari, K.; Rendell, A.; Burant, J. C.; Iyengar, S. S.; Tomasi, J.; Cossi, M.; Rega, N.; Millam, N. J.; Klene, M.; Knox, J. E.; Cross, J. B.; Bakken, V.; Adamo, C.; Jaramillo, J.; Gomperts, R.; Stratmann, R. E.; Yazeyev, O.; Austin, A. J.; Cammi, R.; Pomelli, C.; Ochterski, J. W.; Martin, R. L.; Morokuma, K.; Zakrzewski, V. G.; Voth, G. A.; Salvador, P.; Dannenberg, J. J.; Dapprich, S.; Daniels, A. D.; Farkas, Ö.; Foresman, J. B.; Ortiz, J. V.; Cioslowski, J.; Fox, D. J. *Gaussian 09*, revision A.02; Gaussian, Inc.: Wallingford, CT, 2009.
- Scalmani, G.; Frisch, M. J. *J. Chem. Phys.* **2010**, *132*, 114110.

- (40) Purvis, G. D.; Bartlett, R. J. *J. Chem. Phys.* **1982**, *76*, 1910–1918.
(41) Stanton, J. F.; Gauss, J.; Harding, M. E.; Szalay, P. G. CFOUR, a quantum chemical program package, 2010, <http://www.cfour.de>.
(42) Schuchardt, K. L.; Didier, B. T.; Elsethagen, T.; Sun, L. S.; Gurumoorthi, V.; Chase, J.; Li, J.; Windus, T. L. *J. Chem. Inf. Model.* **2007**, *47*, 1045–1052.
(43) Wolinski, K.; Hinton, J. F.; Pulay, P. *J. Am. Chem. Soc.* **1990**, *112*, 8251–8260.
(44) Gauss, J.; Stanton, J. F. *J. Chem. Phys.* **1995**, *102*, 251–253.
(45) Gauss, J.; Stanton, J. F. *J. Chem. Phys.* **1995**, *103*, 3561–3577.
(46) Sychrovský, V.; Grafenstein, J.; Cremer, D. *J. Chem. Phys.* **2000**, *113*, 3530–3547.
(47) Helgaker, T.; Watson, M.; Handy, N. C. *J. Chem. Phys.* **2000**, *113*, 9402–9409.
(48) Auer, A. A.; Gauss, J. *Chem. Phys.* **2009**, *356*, 7–13.
(49) Florián, J.; Štrajbl, M.; Warshel, A. *J. Am. Chem. Soc.* **1998**, *120*, 7959–7966.
(50) Kyogoku, Y.; Iitaka, Y. *Acta Crystallogr.* **1966**, *21*, 49.
(51) Gorenstein, D. G.; Luxon, B. A. *Biochemistry* **1979**, *18*, 3796–3804.
(52) Barbic, A.; Zimmer, D. P.; Crothers, D. M. *Proc. Natl. Acad. Sci. U.S.A.* **2003**, *100*, 2369–2373.
(53) Lankhorst, P. P.; Haasnoot, C. A. G.; Erkelens, C.; Altona, C. J. *Biomol. Struct. Dyn.* **1984**, *1*, 1387–1405.
(54) Plavec, J.; Chattopadhyaya, J. *Tetrahedron Lett.* **1995**, *36*, 1949–1952.